Structural Basis of the Broad Specificity of a General Odorant-Binding Protein from Honeybee

Ewen Lescop,[‡] Loïc Briand,[§,||] Jean-Claude Pernollet,[§] and Eric Guittet*[,‡]

Laboratoire de Chimie et Biologie Structurales, Institut de Chimie des Substances Naturelles, CNRS UPR 2301, 1 avenue de la Terrasse, 91190 Gif-sur-Yvette, France, and INRA, UMR1197 Neurobiologie de l'Olfaction et de la Prise Alimentaire, Biochimie de l'Olfaction et de la Gustation, 78352 Jouy-en-Josas, France

Received December 17, 2008; Revised Manuscript Received February 2, 2009

ABSTRACT: General odorant-binding proteins (GOBPs) are believed to transport a wide range of volatile hydrophobic molecules across the aqueous sensillum lymph toward olfactory receptors in insects. GOBPs are involved in the first step of odorant recognition, which has a great impact in agriculture and in insect-mediated human disease control. We report here the first structural study of a GOBP, the honeybee ASP2, in complex with a small hydrophilic ligand. The overall fold of the NMR structure of ASP2 consists of the packing of six α-helices creating an internal cavity and closely resembles that of the related pheromone-binding proteins (PBPs). The predominantly hydrophobic internal cavity of ASP2 provides additional possible interactions (π-stacking, electrostatic contact) for ligand binding. We also show that the internal cavity of ASP2 has the ability to bind ligands of different structures and properties, including a hydrophobic component of the floral scent [2-isobutyl-3-methoxypyrazine (IBMP)] and a small hydrophilic ligand. We further demonstrate that IBMP binds ASP2 with two stable alternative conformations inside the ASP2 binding pocket. The ^{15}N NMR relaxation study suggests that significant backbone mobility occurs at the ligand entry site at the millisecond rate, which likely plays a role in the recognition and the uptake−release mechanism of ligands by ASP2. We propose that the broad ligand specificity of GOBPs compared with PBPs is conferred by the cumulative effects of weak nonspecific protein−ligand interactions and of enhanced protein internal dynamics at the ligand entry site.

In insect antennae, the first step in chemical detection is the transport of airborne hydrophobic signaling molecules by odorant-binding proteins (OBPs)[1] to receptor neurons through the sensillum lymph (*1*−*4*). Insect OBPs are small acidic soluble proteins (13−16 kDa), highly concentrated in the sensillum lymph. They can be roughly classified as general odorant-binding proteins (GOBPs), pheromone-binding proteins (PBPs), and chemosensory proteins (CSPs) (*1*−*4*). On one hand, GOBPs are thought to play a general role in olfaction by carrying diverse odorant molecules such as plant volatiles and are expressed in both males and females. On another hand, PBPs are supposed to be tuned to sex pheromone detection and are mostly specific to male antennae. The role of CSPs is less documented. However, they have been shown to bind a wide range of chemicals involved in insect chemical communication (*4*). In spite of a low degree of amino acid sequence homology, insect PBPs and GOBPs possess three conserved disulfide bridges, whereas CSPs share no structural similarity with PBPs and GOBPs. Although the physiological function of OBPs is not yet well understood, their essential role in eliciting the behavioral response and odor coding has been demonstrated (*5*−*10*). The growing amount of evidence for the implication of OBPs in animal behavior indicates that additional research should be carried out in an effort to better characterize their precise function(s) at a molecular level. Several nonexclusive functional roles have been proposed in the past (*1, 2*). GOBPs and PBPs may be involved in the passive transport of odorants through the sensillum lymph, in odorant-specific recognition, in the control of extracellular odorant concentration together with specific degrading enzymes, in odorant sequestration after signal transduction, or in the direct interaction of the protein−ligand complex with olfactory receptors for signal transduction (*1, 2*).

Since their discovery in several Lepidoptera moths (*11*−*14*), and despite their important role in eliciting odor-guided insect behavior (*8*), GOBPs have received little attention compared with PBPs. The binding properties of GOBPs are poorly documented, although, in Lepidoptera, GOBPs have been shown to bind plant odors and also pheromones or antagonists (*15, 16*). Due to the crucial role of the honeybee in the ecosystem and agronomy, we have been focusing our efforts on studying OBPs from *Apis mellifera* L. We have described in this species the GOBP ASP2 protein together

* To whom correspondence should be addressed: Laboratoire de Chimie et Biologie Structurales, ICSN-CNRS UPR2301, 1 avenue de la Terrasse, 91190 Gif-sur-Yvette, France. Phone: +33.1.69.82.37.97. Fax: +33.1.69.82.37.84. E-mail: eric.guittet@icsn.cnrs-gif.fr.

‡ CNRS UPR 2301.

§ INRA.

|| Present address: INRA, UMR1129 FLAVIC, F-21000 Dijon, France.

[1] Abbreviations: CPMG, Carr−Purcell−Meiboom−Gill; CSP, chemosensory protein; GOBP, general odorant-binding protein; HSQC, heteronuclear single-quantum correlation; IBMP, 2-isobutyl-3-methoxypyrazine; NOESY, nuclear Overhauser effect spectroscopy; OBP, odorant-binding protein; PBP, pheromone-binding protein; rmsd, root-mean-square deviation; TSP, 3-trimethylsilylpropionate-2,2,3,3-d_4.

10.1021/bi802300k CCC: $40.75
Published on Web 02/02/2009

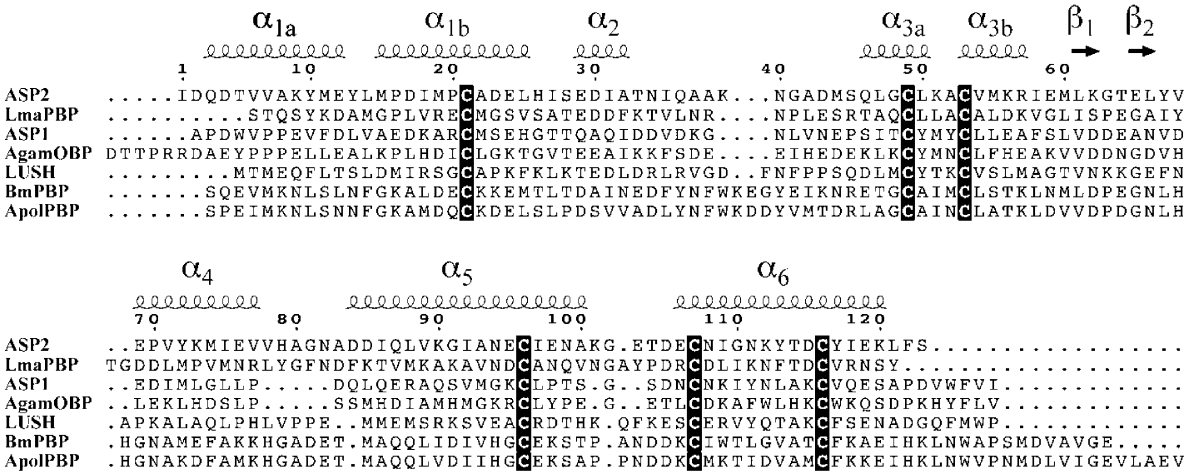

FIGURE 1: Multiple-sequence alignment of odorant-binding proteins. The plot shows the structure-based multiple-sequence alignment of OBPs: honeybee GOBP ASP2, *Leucophaea maderae* LmaPBP, honeybee PBP ASP1, *Anopheles gambiae* AgamOBP1, *Drosophila melanogaster* LUSH, *Bombyx mori* BmPBP, and *Antheraea polyphemus* ApolPBP. Strictly conserved cysteine positions are highlighted. The secondary structures of ASP2 are represented at the top. This figure was prepared with ESPript (*59*).

with PBP ASP1 and CSP ASP3 (*17*). ASP2 does not bind any molecule of the queen pheromone blend but was shown to bind several classes of odorants (*18*). Because of its homology in amino acid sequence with OBPs, including the three conserved disulfide bridges (Figure 1), its expression in both workers and drones, its location in sensilla (*19*), and its binding properties (*18*), the 123-amino acid ASP2 was consequently classified as a GOBP. Very few insect GOBPs, including ASP2, have been demonstrated to have unambiguous binding specificity for host plant components (*18*). Therefore, ASP2 represents an excellent model of GOBP for understanding the molecular basis for the different ligand specificity of GOBPs and PBPs.

A wealth of high-resolution structural information is already available for PBPs from various species (reviewed in refs *3* and *4*). In contrast, no structural information has been gathered yet concerning proteins from the GOBP subfamily, while they are involved in the essential task of plant recognition. To obtain the first structural characterization of a GOBP and to provide a structure-based rationale for the distinct binding properties of GOBPs and PBPs, we determined the solution NMR structure of ASP2 in complex with the TSP molecule, a small hydrophilic ligand. Interestingly, the honeybee ASP2 structure shows closer features with the cockroach *Leucophaea maderae* LmaPBP than with PBP ASP1 from honeybee. We also studied the ASP2 protein backbone dynamics by ^{15}N NMR relaxation and the interaction of ASP2 with IBMP, a component of the floral scent (*20*). We propose that the broadening of the ligand binding range of ASP2 compared with PBPs may be explained by the cumulative effects of the high versatility of the binding pocket and the enhanced mobility at the entry site of the GOBP.

EXPERIMENTAL PROCEDURES

Sample Preparation and NMR Spectroscopy. Singly ^{15}N-labeled and doubly ^{15}N- and ^{13}C-labeled proteins were heterogeneously secreted by the yeast *Pichia pastoris* and purified by reversed phase chromatography as previously described (*21*). NMR samples contained 0.5−1 mM uniformly ^{15}N-labeled or ^{13}C- and ^{15}N-labeled ASP2, 30 mM TSP, 100 mM sodium phosphate (pH 6.0), 0.02% (w/v) sodium azide, and a 90% H_2O/10% D_2O mixture, unless otherwise specified. NMR spectra for resonance assignment and structure calculations were acquired on a Bruker 800 MHz spectrometer equipped with a triple-resonance *z*-axis gradient probe. ASP2 backbone ^{1}H, ^{15}N, and ^{13}C resonances were previously assigned at 308 K in complex with TSP using standard three-dimensional (3D) triple resonance (*22*). The assignment was further extended to side chain resonances by analyzing 3D ^{15}N-edited TOCSY and 3D ^{13}C-edited HCCH-TOCSY spectra. NOE-derived distance restraints were extracted from a 3D ^{15}N-edited NOESY spectrum (τ_m = 150 ms), a 3D ^{13}C-edited NOESY spectrum (τ_m = 120 ms) in a 90% H_2O/10% D_2O mixture, and a two-dimensional (2D) NOESY spectrum (τ_m = 100 ms) in a 90% D_2O/10% H_2O mixture at 308 K. Side chain ^{1}H, ^{13}C, and ^{15}N resonances of ASP2 in complex with TSP were fully assigned, except for I18, K39, K51, and Q87 due to overlapping and/or low-intensity signals. Backbone ϕ angles were extracted from a HNHA experiment (*23*). Amide hydrogen exchange was assessed using a series of ^{15}N HSQC spectra after the addition of 100% D_2O to a lyophilized protein powder. NMR data processing was achieved using NMRPipe and NMRDraw (*24*) and analyzed using NMRView (*25*).

Structure Calculations and Analysis. TALOS (*26*) was used to predict the backbone dihedral angles of 86 amino acids. Thirty-seven hydrogen bonds were identified in helices from the ^{1}H−^{2}H exchange experiments and analysis of the initial structures. An automatic NOE assignment strategy was performed using ARIA 1.2 (*27*) in combination with CNS 1.1 (*28*). The topology and parameter files for TSP were generated using XPLO2D (*29*). The structure calculation of ASP2 was initially carried out without the distance restraints involving TSP to prevent distortion of the protein conformation during the automated NOE assignment steps. When reasonable structures of ASP2 were obtained, the intermolecular restraints were included assuming equimolar stoichiometry between ASP2 and TSP (1:1 complex). The 17 lowest-energy structures were conserved for analysis by PROCHECK (*30*) and MOLMOL (*31*). MOLMOL and

PyMOL (*32*) were used to prepare the pictures of the structures. The structure of ASP2 was compared to a structure database using the server DALI (*33*).

^{15}N Relaxation Measurements. ^{15}N R_1, R_2, and heteronuclear $\{^1H\}-^{15}N$ NOE relaxation parameters were extracted from sensitivity-enhanced pulse sequences (*34*) on a Bruker 600 MHz Avance spectrometer equipped with a triple-resonance *z*-axis gradient probe. The relaxation delays for the R_1 experiments were 12, 48, 72 (×2), 128, 300, 420, 600, 840, and 1200 ms (in random order), using a recycle delay of 4 s. For the R_2 experiments, the delays were 8, 16, 32, 48 (×2), 64 (×2), 136, 256 (×2), and 400 ms (in random order) and the τ_{CP} delay (delay between two ^{15}N inversion pulses during the CPMG scheme) was set to 1 ms. For the heteronuclear $\{^1H\}-^{15}N$ NOE measurements, two spectra were acquired with and without proton saturation during 5 s. The R_1 and R_2 rates and heteronuclear NOE values and their associated errors were determined from the peak intensities using the routines in NMRView. Relaxation parameters were then interpreted in terms of atomic motion by TENSOR2 (*35*) in the framework of the Model-Free formalism (*36, 37*). The isotropic tumbling model was selected since no improvement was found with the anisotropic model. Chemical exchange processes were probed by using the CPMG-based relaxation compensated pulse sequence developed by Loria et al. (*38*). Two experiments were carried out with τ_{CP} delays of 0.63 and 6.18 ms. The chemical exchange contribution (R_{ex}) to the transverse relaxation rate was estimated from the total duration of the CPMG sequences ($T = 50$ ms) and the ratio in intensities in both experiments.

NMR Binding Experiment. The assignment of the resonances of free IBMP in a 90% D_2O/9.5% H_2O/0.5% methanol mixture was carried out at 308 K with one-dimensional (1D) spectra and 2D NOESY spectra (Figure S1 of the Supporting Information). A sample of 0.3 mM ^{15}N-labeled ASP2 [100 mM sodium phosphate, 0.02% (w/v) NaN_3, and 90% H_2O/10% D_2O (pH 6.0)] was titrated with a stock aqueous solution of 40 mM IBMP in 0.5% (v/v) methanol. Methanol was used to help the solubilization of IBMP in H_2O, and the inability of ASP2 to bind methanol was checked by the absence of perturbation of the ^{15}N HSQC spectrum of the protein upon addition of a 2:1 methanol/ASP2 molar excess. The IBMP:ASP2 molar ratio was adjusted from 0 to 1.66 in 0.33 steps. The titration was monitored by 1D ^{15}N-filtered, 2D ^{15}N-filtered NOESY, and ^{15}N HSQC spectra. Resonance assignment of ASP2 in complex with IBMP was straightforward through the analysis of ^{15}N-edited NOESY spectra and the comparison with chemical shift values of ASP2 in complex with TSP. The structural models for the ASP2·IBMP complex were built as follows. The TSP molecule was removed in one representative structure of the ASP2·TSP complex and replaced by one (models A and B) or two molecules (model C) of IBMP. Then, an ensemble of structures of the ASP2·IBMP complex was calculated using the simulated annealing protocol in CNS. All restraints used for the ASP2·TSP complex were included in the calculation to restrain the protein conformation, except that the intermolecular ASP2·TSP restraints were replaced by the intermolecular ASP2·IBMP NOE-derived restraints. All calculations were conducted with CNS (*28*). One structure of low total energy was selected to represent each structural model.

Table 1: Structural Statistics for the NMR Structure of the ASP2·TSP Complex

no. of distance restraints[a]	
intraresidual NOE ($\|i-j\|=0$)	1141
interresidual medium-range NOE ($1 \le \|i-j\| \le 4$)	1093
interresidual long-range NOE ($\|i-j\|>4$)	469
unambiguous NOE	2027
ambiguous NOE	321
total NOE-based restraints	2348
total hydrogen bonds distances[b]	74
ensemble rmsd (Å)[c]	
secondary structure (backbone) except helix α_2	0.85 ± 0.19
secondary structure (heavy) except helix α_2	1.43 ± 0.23
backbone (residues 1−25 and 47−123)	1.01 ± 0.20
heavy atoms (residues)	1.50 ± 0.22
all backbone atoms	1.58 ± 0.41
all heavy atoms	2.10 ± 3.06
no. of violations (experimental restraints)[a]	
NOEs and H-bonds (>0.3 Å)	1
dihedral angles (deg)	1
rmsd (experimental restraints)[a]	
NOEs (Å)	0.027 ± 0.001
H-bonds (Å)	0.014 ± 0.004
dihedral angles (deg)	0.78 ± 0.60
rmsd (covalent restraints)[a]	
bonds (Å)	0.0017 ± 0.0002
angles (deg)	0.34 ± 0.03
improper angles (deg)	0.26 ± 0.04
Ramachandran spaces (%)[d]	
most favored	80.0 ± 2.6
additionally allowed	17.8 ± 2.4
generously allowed	1.7 ± 1.0
disallowed	0.5 ± 0.5

[a] Output by ARIA. [b] Thirty-seven hydrogen bonds with two distance restraints. [c] Calculated with MOLMOL. [d] Calculated with PROCHECK.

Data Deposition. The coordinates of the structure of the ASP2·TSP complex have been deposited in the Protein Data Bank (PDB) (entry 1TUJ).

RESULTS

The Structure of ASP2 Was Determined in Complex with TSP. In the absence of ligand, ASP2 was globally well folded at pH 6, as indicated by the high $^1H/^{15}N$ chemical shift dispersion in the ^{15}N HSQC spectrum. However, many cross-peaks in the ^{15}N HSQC spectrum were doubled and/or broadened, and no homogeneous spectrum could be obtained while the pH was varied in the range of 4−8. This is indicative of important conformational heterogeneity of apo-ASP2 under these conditions, which would severely have hampered the structural study of ASP2. Initial studies also showed that in a 30:1 excess of the partially deuterated TSP molecule (3-trimethylsilylpropionate-2,2,3,3-d_4), commonly used as an internal reference for NMR chemical shifts, all residues of ASP2 were represented at pH 6 by a unique correlation peak in the spectra, except G48 and L50 for which multiple cross-peaks were still present. The interaction between ASP2 and TSP was further confirmed by the observation of several intermolecular NOEs involving the protonated trimethylsilyl group of TSP and residues forming the binding cavity of ASP2. Because of the spectral homogeneity of ASP2 in complex with TSP, the structural and dynamic studies of ASP2 were then carried out with a molar excess of 30:1 of TSP at pH 6.

Overall Structure of ASP2. Table 1 sums up the extension of NOE assignments, the energy parameters of the 17 lowest-energy structures of the ASP2·TSP complex, and the

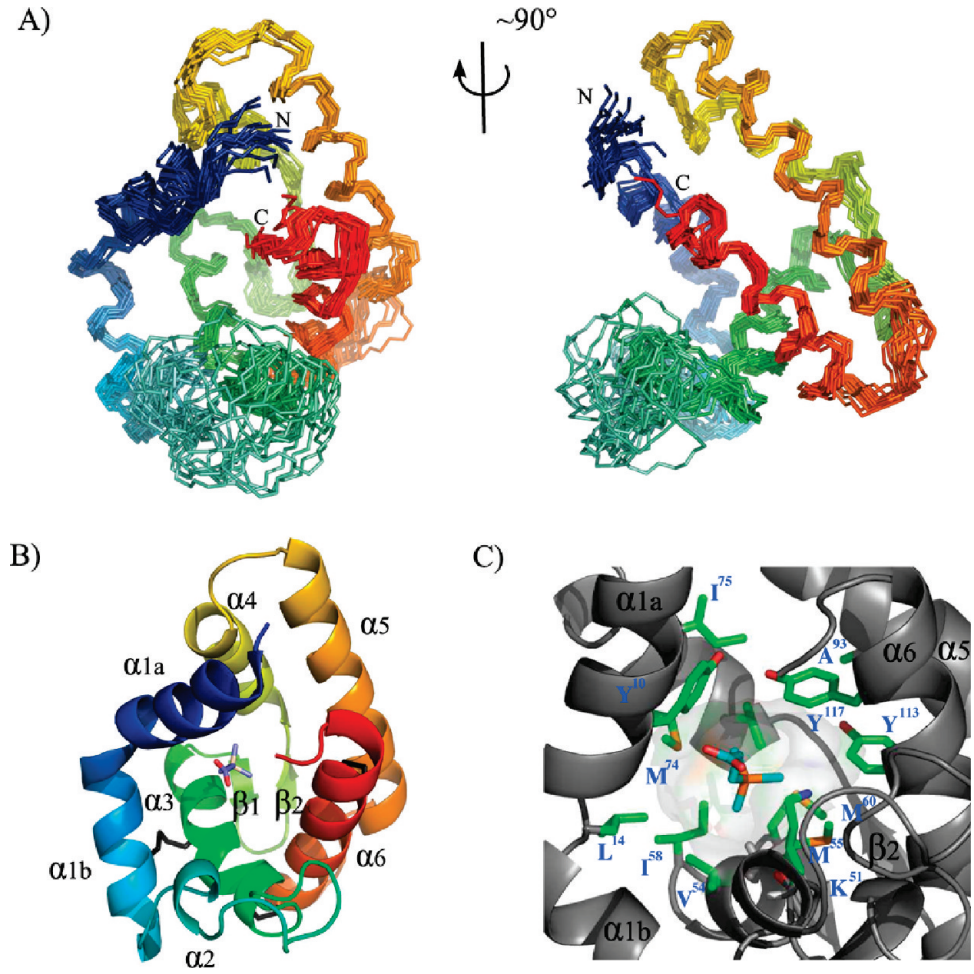

FIGURE 2: Structure of the ASP2·TSP complex. (A) Views of a superimposition of the 17 selected conformers of ASP2 in complex with TSP. The left and right views have approximately ~90° relative orientations. The N- and C-terminal extremities are labeled. (B) Ribbon representation of the selected conformer of the ASP2·TSP complex. The three disulfide bridges are represented as black sticks, and the TSP molecule is shown as sticks and colored by atoms. The secondary structures are labeled. (C) View of TSP in the binding pocket of the selected conformer. TSP (colored by atoms) is represented as sticks. The ASP2 protein is represented as gray ribbons. The semitransparent surface denotes the inner cavity delineated by amino acids shown by green sticks and labeled in blue.

geometric properties of the ensemble of structures, represented in Figure 2A. One of the 17 structures was selected (Figure 2B) as a good representative of the ensemble on the basis of a low global energy and a low backbone rmsd toward the mean structure. The secondary structure of ASP2 mainly consists of six α-helices, two of them being significantly disrupted: α_{1a} (residues 3−13), α_{1b} (residues 15−25), α_2 (residues 29−32), α_{3a} (residues 47−50), α_{3b} (residues 53−57), α_4 (residues 69−77), α_5 (residues 84−100), and α_6 (residues 106−120) (Figure 2B). The arrangement of the helices is essentially fixed by the three disulfide bridges (C21−C53, C49−C107, and C96−C116) and closely resembles that of the structures of PBPs. Briefly, helices α_1, α_4, α_5, and α_6 converge to form the top of a cone capped at the other extremity by helix α_3. The D25−S45 fragment, which encompasses helix α_2 and the $\alpha_2-\alpha_{3a}$ loop, is much less well defined than the other regions of the structure, as indicated by the higher rmsd in this region (Figure 3A). This reflects the absence of long-range restraints and the scarcity of medium-range restraints for residues S28−S45. As a consequence, helix α_2 and the $\alpha_2-\alpha_{3a}$ loop are loosely packed toward the core of the structure (Figure 2A).

Internal Cavity of ASP2. The helix packing of ASP2 creates an internal cavity of roughly spherical shape (radius of 7−8 Å) (Figure 2C). The inner surface of the cavity contains contributions of amino acids belonging to all helices except helix α_2 and is delineated by many hydrophobic side chains (L14, V54, M55, I58, M60, V71, M74, I75, and A93), a few polar noncharged side chains (Y10, Y113, T114, Y117, and S123), and one positively charged side chain (K51). This distribution creates a hydrophobic patch at the bottom of the cavity (helices α_{3b}, α_4, and α_5) and a polar environment near the opening of the cavity (helices α_1 and α_6). The cavity is largely accessible to the solvent through a mouth present in all of the structures. The side chains of Y10, L14, V54, Y117, and S123 form the mouth. The internal cavity is thus opened on a wide surface of the protein. Since no other significant opening is present on the structure of ASP2, this mouth is likely the entry−exit site of the ligands. Six unambiguous NOE contacts were identified between the methyl groups of TSP and side chains at the bottom of the cavity of ASP2, including the aromatic protons of tyrosines 10, 113, and 117 and the methyl group of M74. This NOE information together with the NMR ensemble suggests that the trimethylsilyl group of TSP points toward the bottom of the cavity and that the acidic group of TSP points toward the ligand entry site. The observed orientation of the TSP ligand inside the cavity can be explained on one hand by the favorable van der Waals interactions between the trimethylsilyl group of

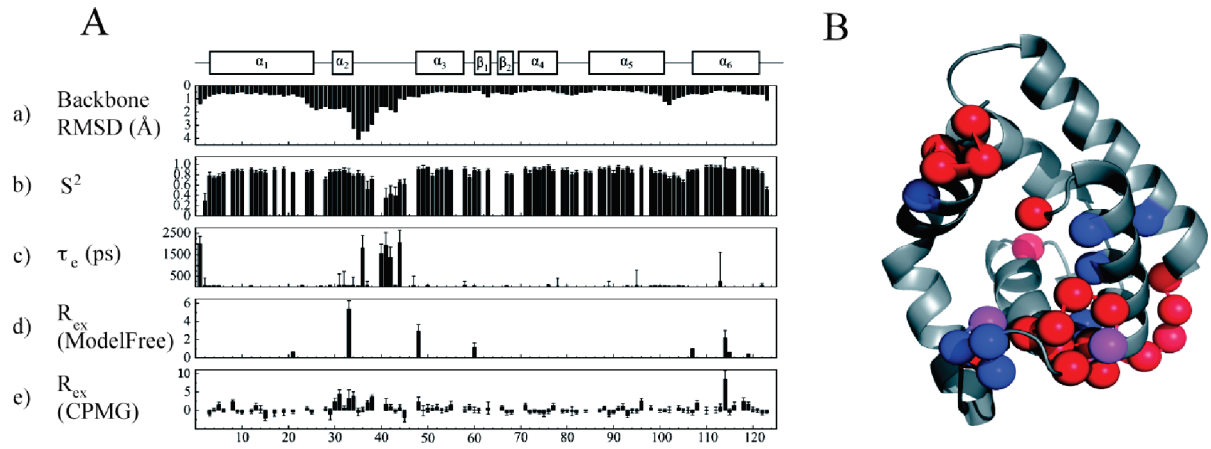

FIGURE 3: Model-Free parameters of ASP2 in complex with TSP. The microdynamics parameters obtained at 308 K are shown in panel A: (a) local backbone rmsd from the mean structure, (b) squared order parameter S^2, (c) internal correlation time τ_e, derived from Model-Free analysis, and (d and e) conformational exchange terms (R_{ex}) derived from Model-Free analysis and CPMG experiments, respectively. The secondary structures are represented at the top of panel A. In panel B, the flexible residues are mapped onto the representative structure of the ASP2·TSP complex. Residues with fast internal dynamics of significant amplitude ($S^2 < 0.8$) or with significant conformational exchange as judged from Model-Free or CPMG methods (see the text) are represented as red and blue spheres, respectively. Residues with both fast dynamics and conformational exchange are represented as magenta spheres.

TSP and the hydrophobic bottom of the ASP2 cavity and on another hand by the electrostatic interactions between the acidic group of TSP and the negatively charged side chain of K51.

Backbone Flexibility at the Ligand Entry Site. The ^{15}N R_1, R_2, and $\{^1H\}-^{15}N$ heteronuclear NOE values of ASP2 in complex with TSP were measured at a ^1H frequency of 600 MHz at 308 K. The overall correlation time (τ_c) estimated from the R_2/R_1 ratios was 4.87 ± 0.04 ns, consistent with a monomeric state of ASP2 under these conditions (*39*). Model-Free analysis of NMR relaxation data provides a wealth of information in terms of internal mobility and time scales of these motions. Such a description of motions is reflected by the squared order parameter (S^2), the internal correlation time (τ_e), and the chemical exchange contribution (R_{ex}) to the transverse relaxation (R_2). The mean squared order parameter (S^2) (0.85) calculated on the secondary structures of ASP2 was consistent with a globally well structured protein (Figure 3B). Motions of significant amplitude ($S^2 < 0.8$) were found at the N- and C-terminal extremities (D2−T5 and S123) and in loops linking secondary structures (S28, E59, and G102 to D105). Of interest, the squared order parameters for residues spanning A37−S45 (mean S^2 of 0.52) were also significantly lower than average, and internal correlation times (τ_e) corresponding to relaxation-effective motions in the nanosecond time scale had to be introduced for these residues to fit the relaxation data. Significant chemical exchange contributions (higher than 2 s^{-1}) had to be introduced for three amino acids: T33, G48, and T114 (Figure 3D). The CPMG relaxation dispersion experiment is sensitive to chemical exchange occurring at the millisecond rate (Figure 3E). On the arbitrary criterion "R_{ex} higher than 1.5σ", where σ is the standard deviation of R_{ex} over the sequence, 10 residues (A8, D30, I31, T33, N34, A38, G48, C96, T114, and I118) were identified as experiencing significant chemical exchange on the millisecond time scale.

It is worth noting that most residues in the ill-defined region of the ensemble of NMR structures experienced significant internal mobility on the pico- to nanosecond time scales (around the $\alpha_2-\alpha_{3a}$ loop) and/or at the millisecond time scale (around helix α_2). Therefore, the high rmsd values in helix α_2 and in the $\alpha_2-\alpha_{3a}$ loop in the NMR structures reflect the intrinsic backbone flexibility of this region on different time scales. Despite the small amplitude, chemical exchange contributions identified in the CPMG-type experiments corresponded systematically to residues clustering on the protein surface surrounding the ligand entry site. This observation strongly suggests that a concerted dynamic phenomenon occurs at the ligand entry site on the millisecond time scale. Due to the putative loose binding of TSP, this phenomenon could be interpreted as the fast entry or exit of TSP in ASP2. Assuming a two-site exchange model and considering the residue independence of such an exchange mechanism, a linear correlation would be expected between the residue-specific R_{ex} value and the square of the ^{15}N chemical shift difference in the apo and TSP-bound forms. Such correlation was not observed. We concluded that the observed millisecond time scale conformational exchange essentially reflects the intrinsic flexibility of the ASP2·TSP complex that is likely correlated with the opening or closure of the entry site of ASP2.

NMR Binding Experiment with Apo-ASP2 and IBMP. To characterize the location of the binding site(s) of a biologically relevant ligand on ASP2, we studied the binding of IBMP on ASP2. IBMP (Figure 4A) is a green bell pepper odorant and a component of the floral scent (*20*) known to be perceived by honeybees (*40*). An ITC study previously showed that ASP2 binds IBMP in vitro with an affinity in the micromolar range (*18*). To characterize the ASP2−IBMP interaction at the atomic level, we titrated a solution of ^{15}N-labeled apo-ASP2 protein with an increasing amount of IBMP. At each point of the titration, we collected a ^{15}N HSQC spectrum, a ^{15}N-filtered 1D spectrum, and a 2D NOESY ^{15}N-filtered experiment. The ^{15}N-filtered experiments permitted us to monitor the signals of the aromatic hydrogens of IBMP and ASP2 during the titration, while amide hydrogens of the protein were filtered out (see Figure 4B,C). Upon addition of IBMP, two signals of similar intensities were immediately observed at 7.9 ppm (labeled P1a and P1b in Figure 4B). When the IBMP concentration increased, the two resonances P1a and P1b increased in intensity and both converged in the fast exchange regime toward the chemical

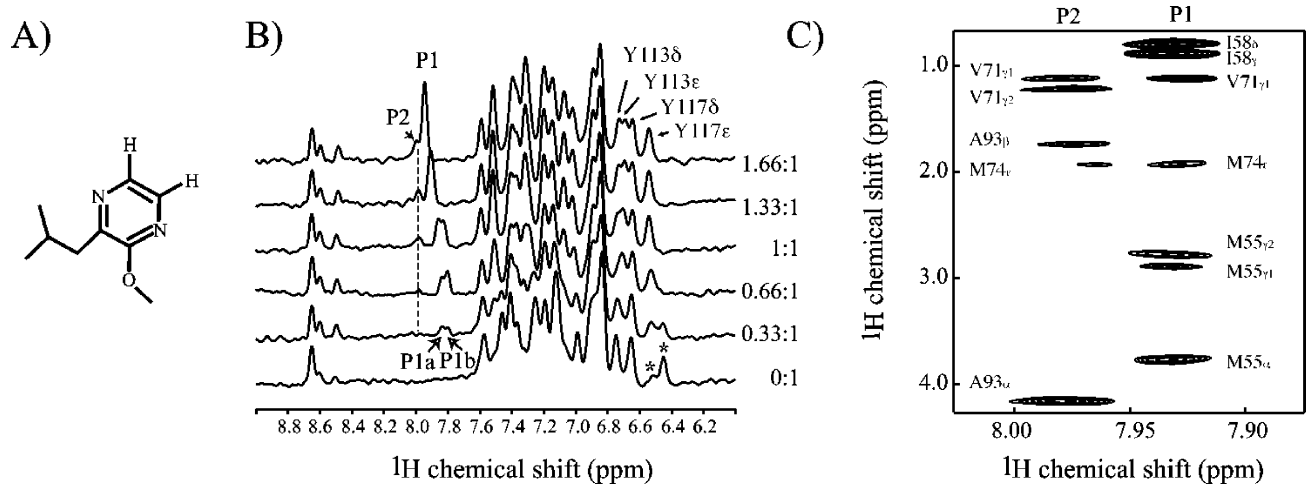

FIGURE 4: Titration of ASP2 by IBMP. (A) Chemical structure of IBMP. (B) ^{15}N-filtered 1D Watergate spectra acquired at IBMP:ASP2 molar ratios ranging from 0:1 to 1.66:1 in 0.33 steps. In these experiments, only aromatic protons are visible. The aromatic resonances of IBMP in the most populated orientation (P1a and P1b) and in the less populated orientation (P2) are labeled. The two asterisks represent the major and the minor resonances of the H_ε atoms of Y117 in the absence of IBMP. The aromatic resonances of residues Y113 and Y117 at the end of the titration are labeled at the top. (C) Close-up view of the ^{15}N-filtered 2D NOESY spectrum recorded at an IBMP:ASP2 molar ratio of 1.66:1 showing the intermolecular NOEs between the aromatic protons of IBMP and the protein. The NOE cross-peaks between the aromatic protons of IBMP in the major (P1) and minor (P2) conformations and the protein resonances are labeled.

shift of the aromatic hydrogens of free IBMP (8.0 ppm). The 2D NOESY experiments showed NOEs between resonances P1a and P1b and several resonances that could be tentatively assigned to hydrogen sites in the binding cavity of ASP2 (side chains of M55, I58, V71, and M74; see Figure 4C). It follows from these observations that resonances P1a and P1b can be unambiguously assigned to the two aromatic hydrogens of one IBMP molecule bound to ASP2 and that these resonances are in fast exchange (on the chemical shift time scale) between the free and ASP2-bound IBMP forms. In addition to resonances P1a and P1b, a signal of weaker intensity (resonance P2) was detected at 8.0 ppm for the IBMP:ASP2 molar ratio of 0.66. Like resonance P1, resonance P2 also increased in intensity with an increasing concentration of IBMP. However, no significant chemical shift variation was observed at higher IBMP concentrations for resonance P2 that was at the same (or indistinguishable) ^{1}H chemical shift as the aromatic hydrogens of free IBMP. The 2D NOESY experiments also showed NOEs between resonance P2 and ^{1}H side chain resonances from the binding pocket of ASP2 (Figure 4C): V71, M74, A93, and Y113. On the basis of these observations, resonance P2 was also assigned to the two aromatic hydrogens (that have degenerate chemical shifts) of IBMP located inside the cavity of ASP2 but in a distinct chemical environment. We interpret the observation of two sets of distinct aromatic resonances for IBMP with different relative intensities involved in different networks of intermolecular NOEs by the existence of (at least) two different binding modes of IBMP in the binding pocket of ASP2. These binding modes may differ by the number, conformation, and/or orientation of the IBMP molecule inside the hydrophobic cavity. We attempted to measure the stoichiometry of the ASP2·IBMP complex using mass spectrometry (ESI-MS). This method was unsuccessful since no complex was observed, likely due to the weak affinity of IBMP for ASP2 [K_d on the micromolar scale (*40*)].

We also investigated the interaction from the point of view of the protein (Figures 4B and 5). In the absence of IBMP, several resonances of ASP2, such as Y117$_\varepsilon$ hydrogens, gave two sets of peaks, consistent with the heterogeneity of apo-ASP2 (vide supra). Upon addition of IBMP, many ASP2 resonances were perturbed. The increasing concentration of IBMP resulted in the complex displacement and intensity changes for the ^{1}H and ^{15}N resonances of ASP2. Two main phenomena were observed. First and for IBMP:ASP2 ratios increasing from 0 and ~1, the major and minor forms of apo-ASP2 decreased and increased in intensity, respectively (see Y117$_\varepsilon$ in Figure 4B and C116 for example in Figure 5). For an IBMP:ASP2 ratio of ~1.0, the major form of apo-ASP2 completely disappeared and a unique cross-peak was observed for the vast majority of ASP2 residues. This observation was consistent with the conformational selection of ASP2 upon IBMP binding and suggested that the minor form of apo-ASP2 is the only one able to bind IBMP. However, one cannot rule out the possible displacement of copurified contaminants by IBMP. In addition to the increase in intensity, a subset of ASP2 cross-peaks also showed small but significant ^{1}H and ^{15}N chemical shifts changes for IBMP:ASP2 ratios higher than 0.7 (e.g., I58, C96, G110, and Y117 in Figure 5). This observation is consistent with the fast equilibrium (on the chemical shift time scale) of ASP2 resonances between the minor form of the apoprotein and the IBMP-bound state(s). The existence of several states of apo-ASP2 and of at least two IBMP-bound states of ASP2 likely explains the complex chemical shift data. In general, the NMR spectra provide a convenient way to extract the relative populations for the various states of a species in solution, either from the relative cross-peak intensities (in the case of slow exchange) or from the population-averaged chemical shifts (in the case of fast exchange). Assuming that the binding event can be unambiguously described by one or several competing equilibria, this information can be used to obtain the thermodynamic constant(s) by data fitting. In our case, the complex binding event and the unknown stoichiometry of the ASP2·IBMP complexes prevented the extraction of the relevant binding affinities.

In the last ^{15}N HSQC spectrum of the experiment, the vast majority of the residues were represented by a unique cross-

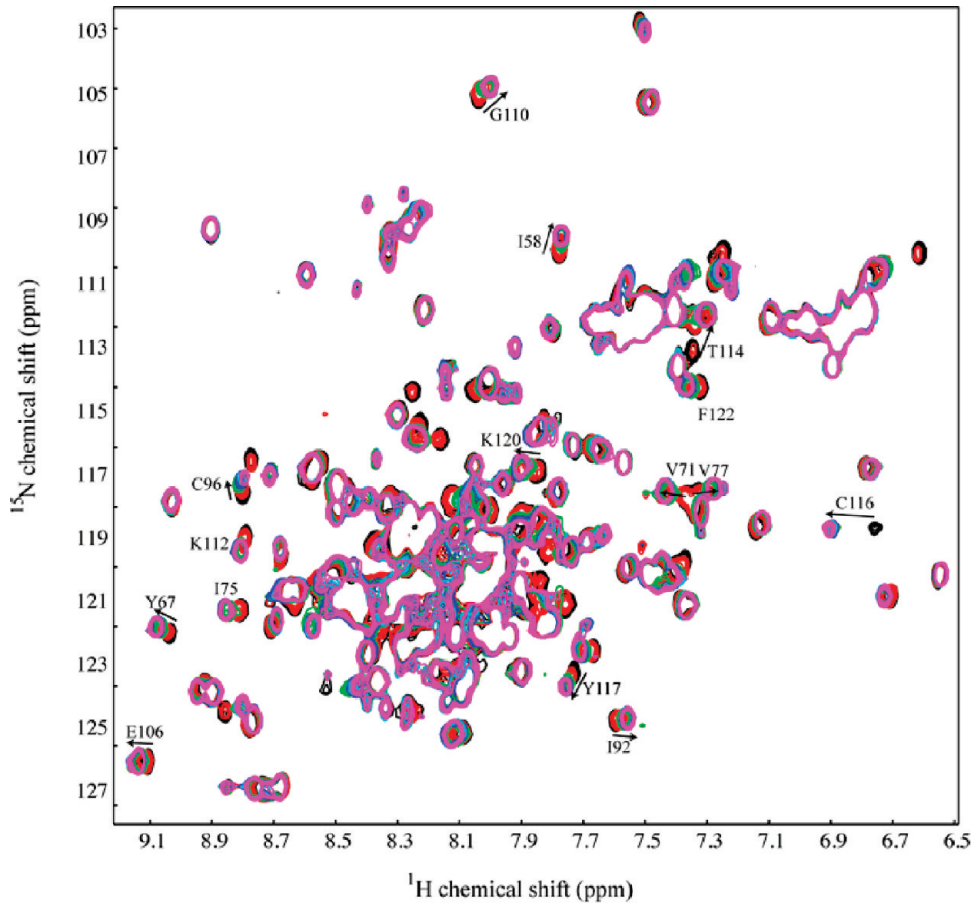

FIGURE 5: ^{15}N HSQC spectra of ASP2 acquired for increasing concentrations of IBMP. The ^{15}N HSQC spectra shown here were recorded at molar ratios (IBMP:ASP2) of 0:1 (black), 0.33:1 (red), 0.66:1 (green), 1:1 (blue), 1.33:1 (cyan), and 1.66:1 (magenta). Residues with significant chemical shift perturbation upon addition of IBMP are labeled.

peak (Figures 4B and 5). When the ^{15}N HSQC spectra of ASP2 in the TSP- and IBMP-bound states were compared, strong similarities were found (Figure S3 of the Supporting Information). This strongly suggests that the overall fold of ASP2 is highly similar when bound to the different ligands. This is further supported by the virtually identical NOE patterns observed from the 3D ^{15}N-edited NOESY spectra collected on the TSP- and IBMP-bound ASP2 samples (data not shown). Significant small differences in ^{1}H and ^{15}N chemical shifts were found for residues lining the binding cavity of ASP2, consistent with the different chemical nature of the embedded ligands (Figure S3 of the Supporting Information). However, the biggest differences in ^{1}H and ^{15}N chemical shifts were found for residues around the C96−C116 disulfide bridge, linking helices α_5 and α_6. This suggests a possible ligand-induced rearrangement of the S−S bond due to the reorientation of the side chains of the neighboring aromatic residues Y113 and Y117, which are exposed inside the binding cavity (Figure S4 of the Supporting Information). Therefore, the ASP2 structure is highly conserved in the different liganded states, although little accommodation likely occurs near the binding cavity to adapt to the size and shape of the ligand.

Structural Models for the ASP2·IBMP Complex. The binding experiment with IBMP and ASP2 revealed a complex mechanism largely deviating from the simple bimolecular ASP2 + IBMP ⇔ ASP2·IBMP binding equilibrium. The complete unambiguous framework for the binding mechanism was not further studied. However, relevant structural information could be retrieved from the intermolecular NOEs detected for the aromatic hydrogens of IBMP. We propose three structural models to account for the observed intermolecular NOEs. For models A and B, we hypothesized that one unique IBMP molecule was bound inside the ASP2 cavity (Figure 6A,B). The conformations of IBMP in models A and B were derived from the intermolecular NOEs detected for resonances P1 and P2, respectively. In model A, the aromatic ring of IBMP makes contacts with the hydrophobic patch of the cavity, whereas the isobutyl and methoxy groups are close to the opening and to the polar environment of the cavity. In model B, the aromatic ring of IBMP creates an aromatic stack with Y113 and Y117, which is stabilized by π-stacking contacts, whereas the isobutyl moiety of IBMP is stabilized by hydrophobic interactions at the bottom of the cavity and the methoxy group contacts a polar environment. We also tried to insert two IBMP molecules into the ASP2 cavity, as recently observed for the *B. mori* PBP (*41*). The ASP2 cavity was found to accommodate the two molecules of IBMP without major steric hindrance. We propose a third structural model (model C) with two IBMP molecules inside the binding cavity (Figure 6C). For model C, all available intermolecular NOEs were included in the calculation, supposing that P1 and P2 resonances were associated each with one of the two IBMP molecules inside the cavity. In model C, the main protein−ligand contacts for the IBMP molecule colored blue (red) are essentially preserved compared with model A (B). The NMR data indicate that IBMP

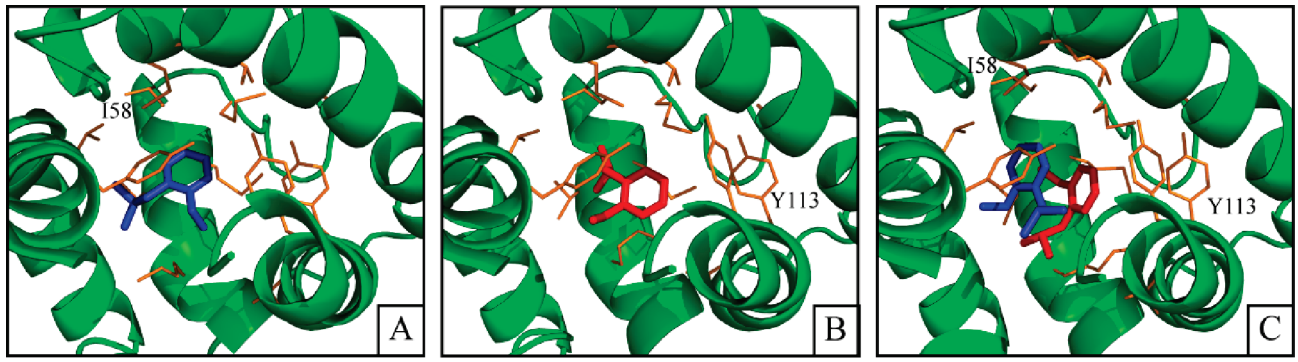

FIGURE 6: Structural models for the ASP2•IBMP complex. In models A and B, one molecule of IBMP is bound inside the cavity of ASP2, whereas model C contains two molecules of IBMP in the ASP2 cavity. The conformations of IBMP molecules colored blue and red were restrained using the intermolecular NOEs observed for resonances P1 and P2, respectively. The protein backbone is represented as green ribbons, and protein side chain delineating the ASP2 cavity are represented as orange sticks.

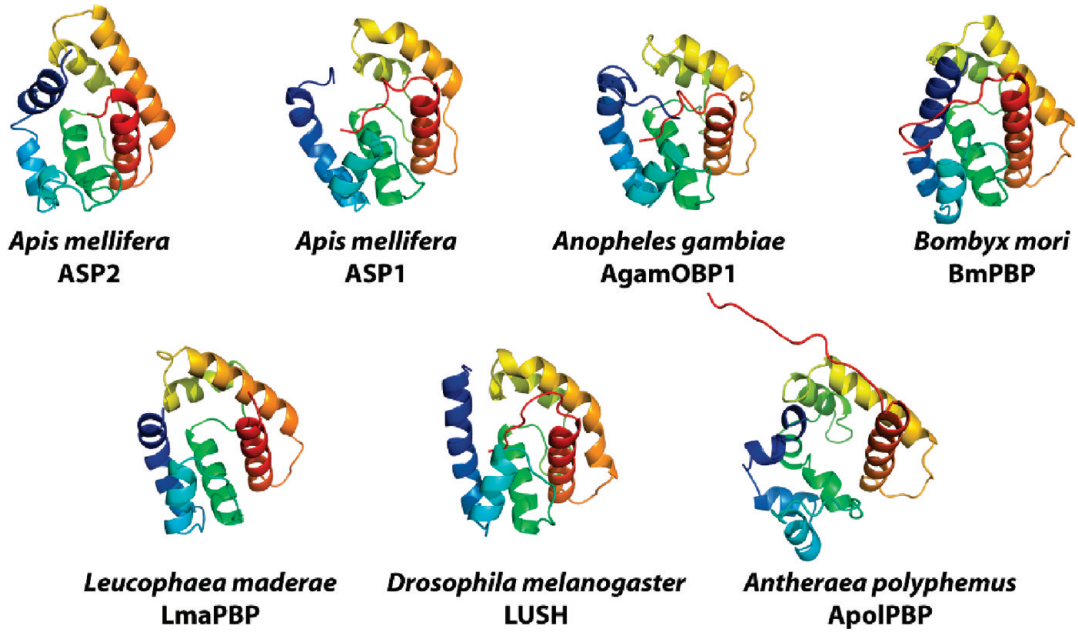

FIGURE 7: Structural comparison of insect OBPs. Ribbon representation of selected structures of OBPs: honeybee *A. mellifera* GOBP ASP2 in complex with TSP (ASP2), cockroach *L. maderae* PBP (LmaPBP, PDB entry 1ORG), honeybee PBP in complex with an additive used in plastics (ASP1, PDB entry 1R5R), *D. melanogaster* OBP in complex with 2-ethanol (LUSH, PDB entry 1OOF), the mosquito *A. gambiae* PBP (AgamOBP1, PDB entry 2ERB), *B. mori* PBP in complex with bombykol (BmPBP, PDB entry 1DQE, chain A), and *A. polyphemus* PBP (ApolPBP, PDB entry 1QWV).

adopts alternative conformations inside the binding cavity of ASP2 which likely share the overall properties of (at least) two of the three proposed structural models. Overall, the intermolecular contacts of ASP2 and IBMP appeared to be mainly driven by hydrophobic, polar, and aromatic stacking interactions. The main result from this analysis is that the ASP2−IBMP interaction cannot be described as a unique binding mode. The binding cavity of ASP2 exposes multiple networks of possible interactions for the stabilization of one molecule of IBMP in multiple stable conformations within the binding cavity.

DISCUSSION

We present here the first high-resolution structure of an insect GOBP, the honeybee ASP2. Its fold consists of a bundle of six α-helices, tightly linked by the three highly conserved disulfide bridges. Interestingly, although having little amino acid sequence identity with PBPs [<16% (Figure 1)] and having different ligand binding properties, the structure of ASP2 can be easily superimposed with those of insect PBPs (*42*−*51*) obtained under near-physiological pH conditions (Figure 7). However, the structures of ASP2 and PBPs differ by significant variations in the orientation of the six α-helices and in the length and conformation of the C-terminal extensions (Figures 1 and 7). This extension has been suggested to be involved in the ligand binding−release mechanism of the PBPs from the moths *B. mori* and *A. polyphemus* through a pH-dependent major conformational change (*44, 52*). However, this C-terminal extension is shorter or even absent in other PBPs, and alternative more classical mechanisms were proposed for other PBPs, such as for the cockroach *L. maderae* LmaPBP (*47*). Overall, the comparison of insect OBP structures shows that the structure of GOBP ASP2 falls into the structural dispersion of PBPs. This is consistent with the idea that the distinct functional

features of GOBP ASP2 with respect to PBPs are not conferred by specific "static" conformational differences.

When structures of PBPs are superimposed on the structure of ASP2 (Figure 7), the most striking similarities are found between ASP2 and LmaPBP (*47*). Indeed, LmaPBP possesses the lowest rmsd value toward the structure of ASP2, as judged by a DALI search (2.6 Å). This mainly reflects the very similar relative positions and orientations of the α-helices in the two structures. In both structures and in contrast with all other PBPs of known structure, the ligand entry sites of ASP2 and LmaPBP are located between helices α_1, α_2, and α_6, which probably correlates well with the absence of the C-terminal extension in both proteins. Finally, LmaPBP and ASP2 share a similar wide profile of possible interactions with the ligands in the binding pocket, including the hydrophobic patch at the bottom of the cavity and the charged environment at the mouth of the cavity. The similarities between ASP2 and LmaPBP likely account for the fact that both proteins can bind hydrophilic as well as hydrophobic ligands and suggest they may share a similar mechanism for the ligand binding and release mechanism (*47, 53*).

It is also of interest to compare the structures of OBPs belonging to the same species. Honeybee ASP1 and ASP2 share only 12% structure-based amino acid sequence identity and have different binding specificities. Whereas ASP1 has been shown to be associated with queen pheromone detection (*54*), ASP2 binds general odorants of diverse chemical nature, but not compounds from the queen pheromone (*18*). Despite having globally similar scaffolds, the structures of the ASP1·*n*-butylbenzene sulfonamide (*42*) and ASP2·TSP complexes show significant differences (Figure 7). The extended C-terminus of ASP1 (eight residues), located after the last helix, folds back and forms one wall of the internal cavity. As a consequence, the N-terminal extremity of the first helix of ASP1 is pushed away toward the solvent when compared to ASP2, and the putative ligand entry sites of ASP2 and ASP1 are located in different positions. In ASP2, the ligand is likely conveyed to the cavity through the wide highly flexible opening delineated by helices α_1, α_2, and α_6. In contrast, a rigid channel permits the entry of the pheromone between helices α_1, α_3, and α_4 in ASP1.

The fact that hymenopteran honeybee ASP2 is structurally closer to the dictyopteran LmaPBP than to honeybee ASP1 deserves two remarks. In insects of different orders, OBPs seemingly converged to a similar ligand release mechanism, though playing different binding roles. In contrast, in a single species, OBPs seem to have functionally diverged by modulations around a common fold. This observation is further supported by the phylogenetic analysis of OBPs (*2*) that indicates that ASP2 is evolutionarily more closely related to LmaPBP (and to lepidopteran PBPs) than to ASP1, which translates into a slightly higher level of sequence identity of ASP2 to LmaPBP (15%) versus ASP1 (12%).

The high specificity of PBPs is thought to be due to the specific interactions between the pheromone and the protein. In contrast, ASP2 is able to accommodate small molecules belonging to different chemical classes, such as IBMP, isoamyl acetate, 1,8-cineol, and 2-heptanone (*18*), in line with its physiological role. On the basis of its structure, the binding versatility of ASP2 can be explained by the variety of chemical groups exposed in the cavity. This variety allows the establishment of different kinds of interactions with ligands, including hydrophobic, polar, electrostatic (through K51), and π-stacking (through Y113 and Y117) interactions. This also provides a rationale for the binding of opportunist ligands, such as TSP, which is a common feature among insect OBPs (*42, 47, 51*). More specific interactions would be expected for natural ligands. Surprisingly, IBMP adopts (at least) two alternative conformations in the cavity of ASP2. These conformations are stabilized by different networks and types of interactions, suggesting weak and nonspecific interactions between ASP2 and IBMP. This is consistent with the relatively high dissociation constant of the ASP2·IBMP complex (micromolar range) (*18*). In contrast to ASP2, the structures of PBPs with their natural ligands exhibit unique ligand binding modes, in line with the model of highly specific pheromone−protein contacts. Interestingly, the binding properties of ASP2 and the vertebrate porcine OBP share common features. In vertebrates, OBPs belong to the lipocalin superfamily and have broad binding specificity toward hydrophobic molecules. Vincent and co-workers observed that the orientations of ligands of various shapes and chemical properties inside the cavity of the porcine OBP were essentially opportunistic (*55*). Although the structures of ASP2 and the porcine OBP are unrelated, their broad specificities are likely based on nonspecific interactions. It should be noted that alternative orientations of a ligand in the binding pocket may counterbalance the weak enthalpy of interaction by a limited increase in entropy during complexation.

Proteins are dynamic systems in nature, and internal motions affect protein function. The ^{15}N relaxation study demonstrated that the internal backbone dynamics of ASP2 are not completely quenched upon complexation with TSP. In particular, the region encompassing the entry site is highly dynamic on the millisecond time scale in the ASP2·TSP complex. Line shape analysis also suggests similar mobility in the ASP2·IBMP complex (data not shown). These slow motions are then likely related to the closure and/or opening or folding and/or unfolding of the ligand entry channel on the millisecond time scale and could be correlated with the uptake−release rate of the ligand. Increased mobility at the entry site of ASP2 may be significant in many aspects. Such flexibility may (i) facilitate the recognition and the progression of the ligand toward the cavity, (ii) increase the rates at which ligands can be recognized and thus accelerate the random process of hydrophobic molecule solubilization for odorant uptake by the insect, (iii) limit the entropy cost for complexation, and (iv) contribute ultimately to the recognition by the cognate olfactory receptors. The internal dynamics of LmaPBP can be evaluated by the temperature factors of the crystallographic structure and thus compared with that of ASP2. Interestingly, residues near the entry site of LmaPBP do not show significantly higher than average Cα *B*-factor values in apo and holo forms. This indicates that the ligand entry site of LmaPBP is mostly rigid. Although the static representations of LmaPBP and ASP2 appear to be very similar, the two proteins show significant different motional behaviors. Internal mobility has been proven to be important in ligand-specific recognition (*56*). Elevated flexibility at the ligand entry site may then contribute to confer a broader specificity to GOBPs when compared to PBPs and may represent a hallmark of GOBPs.

The role of ASP2 in odorant recognition and signal transduction in honeybee can be discussed in light of the results presented here. In the absence of ligand and at near-physiological pH, the structure of ASP2 shows heterogeneity around a common fold. When the ligand binds, the protein is highly stabilized, although the ligand entry site conserved elevated flexibility. Similarly, the LUSH protein is stabilized by alcohols (*57*). The authors proposed that ligand binding could modulate the protein function by stabilizing one conformation of the protein. Such a hypothesis is in agreement with a ligand-specific protein conformational adaptation as observed for LUSH when bound to the pheromone (*10*) and for honeybee PBP ASP1 in complex with various ligands (*58*). In the case of ASP2, the selected conformers upon TSP or IBMP binding are essentially identical with the exception of the subtle structural reorganization near the C96−C116 disulfide bridge, which is likely related to accommodation to ligand size and shape. The similar structural response of ASP2 to biologically irrelevant and relevant ligands does not support the ligand-specific recognition and adaptation for the ASP2 protein required for the ligand-specific activation of olfactory receptors by the GOBP−ligand complex. However, a ligand-specific subtle conformational change was sufficient to exert activation of the olfactory receptor for the LUSH protein (*10*). It is also possible that the protein conformer selected in a non-ligand-specific manner may be recognized by receptors, whereas the flexible apoprotein is not recognized by the receptor. In conclusion, our results supports the non-ligand-specific scavenger role for GOBP ASP2, contributing to the increased concentration of hydrophobic molecules in the sensillum lymph, and/or to the efficient resolubilization of ligands preventing receptor saturation.

Concluding Remarks. The comparison of the averaged structure of ASP2 and PBPs suggests that the differences in the binding properties of PBPs and GOBPs cannot be explained from the static structures. We propose that the broad ligand specificity of GOBPs is due to the weak nonspecific protein−ligand interactions combined with the enhanced internal mobility at the ligand entry site of the GOBP protein.

ACKNOWLEDGMENT

We thank C. van Heijenoort for providing ^{15}N relaxation pulse sequences and for helpful discussions on the interpretation of relaxation data.

SUPPORTING INFORMATION AVAILABLE

NMR study of IBMP free in solution (Figure S1), comparison of the spectra of apo-ASP2 and TSP-bound ASP2 (Figure S2), chemical shift analysis of ASP2 in complex with TSP and IBMP (Figure S3), and a figure highlighting the region between the ligand and the C96−C116 disulfide bridge (Figure S4). This material is available free of charge via the Internet at http://pubs.acs.org.

REFERENCES

1. Pelosi, P. (1996) Perireceptor events in olfaction. *J. Neurobiol. 30*, 13–19.
2. Vogt, R. G. (2005) Molecular basis of pheromone detection in insects. In *Comprehensive Insect Physiology, Biochemistry, Pharmacology and Molecular Biology* (Gilbert, L. I., Iatro, K., and Gill, S., Eds.) pp 753−804, Elsevier, London.
3. Pelosi, P., Zhou, J. J., Ban, L. P., and Calvello, M. (2006) Soluble proteins in insect chemical communication. *Cell. Mol. Life Sci. 63*, 1658–1676.
4. Tegoni, M., Campanacci, V., and Cambillau, C. (2004) Structural aspects of sexual attraction and chemical communication in insects. *Trends Biochem. Sci. 29*, 257–264.
5. Wang, Y., Wright, N. J., Guo, H., Xie, Z., Svoboda, K., Malinow, R., Smith, D. P., and Zhong, Y. (2001) Genetic manipulation of the odor-evoked distributed neural activity in the *Drosophila* mushroom body. *Neuron 29*, 267–276.
6. Krieger, M. J., and Ross, K. G. (2002) Identification of a major gene regulating complex social behavior. *Science 295*, 328–332.
7. Xu, P., Atkinson, R., Jones, D. N., and Smith, D. P. (2005) *Drosophila* OBP LUSH is required for activity of pheromone-sensitive neurons. *Neuron 45*, 193–200.
8. Matsuo, T., Sugaya, S., Yasukawa, J., Aigaki, T., and Fuyama, Y. (2007) Odorant-binding proteins OBP57d and OBP57e affect taste perception and host-plant preference in *Drosophila sechellia*. *PLoS Biol. 5*, e118.
9. Grosse-Wilde, E., Gohl, T., Bouche, E., Breer, H., and Krieger, J. (2007) Candidate pheromone receptors provide the basis for the response of distinct antennal neurons to pheromonal compounds. *Eur. J. Neurosci. 25*, 2364–2373.
10. Laughlin, J. D., Ha, T. S., Jones, D. N., and Smith, D. P. (2008) Activation of pheromone-sensitive neurons is mediated by conformational activation of pheromone-binding protein. *Cell 133*, 1255–1265.
11. Vogt, R. G., Prestwich, G. D., and Lerner, M. R. (1991) Odorant-binding-protein subfamilies associate with distinct classes of olfactory receptor neurons in insects. *J. Neurobiol. 22*, 74–84.
12. Vogt, R. G., Rybczynski, R., and Lerner, M. R. (1991) Molecular cloning and sequencing of general odorant-binding proteins GOBP1 and GOBP2 from the tobacco hawk moth *Manduca sexta*: Comparisons with other insect OBPs and their signal peptides. *J. Neurosci. 11*, 2972–2984.
13. Krieger, J., Ganssle, H., Raming, K., and Breer, H. (1993) Odorant binding proteins of *Heliothis virescens*. *Insect Biochem. Mol. Biol. 23*, 449–456.
14. Krieger, J., von Nickisch-Rosenegk, E., Mameli, M., Pelosi, P., and Breer, H. (1996) Binding proteins from the antennae of *Bombyx mori*. *Insect Biochem. Mol. Biol. 26*, 297–307.
15. Feng, L., and Prestwich, G. D. (1997) Expression and characterization of a lepidopteran general odorant binding protein. *Insect Biochem. Mol. Biol. 27*, 405–412.
16. Jacquin-Joly, E., Bohbot, J., François, M. C., Cain, A. H., and Nagnan-Le Meillour, P. (2000) Characterization of the general odorant-binding protein 2 in the molecular coding of odorants in *Mamestra brassicae*. *Eur. J. Biochem. 267*, 6708–6714.
17. Danty, E., Arnold, G., Huet, J. C., Huet, D., Masson, C., and Pernollet, J. C. (1998) Separation, characterization and sexual heterogeneity of multiple putative odorant-binding proteins in the honeybee *Apis mellifera L. (Hymenoptera: Apidea*). *Chem. Senses 23*, 83–91.
18. Briand, L., Nespoulous, C., Huet, J. C., Takahashi, M., and Pernollet, J. C. (2001) Ligand binding and physico-chemical properties of ASP2, a recombinant odorant-binding protein from honeybee (*Apis mellifera L*). *Eur. J. Biochem. 268*, 752–760.
19. Danty, E., Michard-Vanhée, C., Huet, J. C., Genecque, E., Pernollet, J. C., and Masson, C. (1997) Biochemical characterization, molecular cloning and localization of a putative odorant-binding protein in the honey bee *Apis mellifera L.* (*Hymenoptera: Apidea*). *FEBS Lett. 414*, 595–598.
20. Knudsen, J. T., Tollsten, L., and Bergstroem, L. G. (1993) Floral scents—a checklist of volatile compounds isolated by head-space techniques. *Phytochemistry 33*, 253–280.
21. Briand, L., Lescop, E., Bezirard, V., Birlirakis, N., Huet, J. C., Henry, C., Guittet, E., and Pernollet, J. C. (2001) Isotopic double-labeling of two honeybee odorant-binding proteins secreted by the methylotrophic yeast *Pichia pastoris*. *Protein Expression Purif. 23*, 167–174.
22. Lescop, E., Briand, L., Pernollet, J. C., Van Heijenoort, C., and Guittet, E. (2001) ^{1}H, ^{13}C and ^{15}N chemical shift assignment of the honeybee odorant-binding protein ASP2. *J. Biomol. NMR 21*, 181–182.
23. Vuister, G. W., and Bax, A. (1993) Quantitative J correlation: A new approach for measuring homonuclear three-bond $J(H_NH_\alpha)$

coupling constants in ^{15}N-enriched proteins. *J. Am. Chem. Soc. 115*, 7772–7777.
24. Delaglio, F., Grzesiek, S., Vuister, G. W., Zhu, G., Pfeifer, J., and Bax, A. (1995) NMRPipe: A multidimensional spectral processing system based on UNIX pipes. *J. Biomol. NMR 6*, 277–293.
25. Blevins, R. A., and Johnson, B. A. (1994) NMRView: A computer program for the visualization and analysis of NMR data. *J. Biomol. NMR 4*, 603–614.
26. Cornilescu, G., Delaglio, F., and Bax, A. (1999) Protein backbone angle restraints from searching a database for chemical shift and sequence homology. *J. Biomol. NMR 13*, 289–302.
27. Linge, J. P., O'Donoghue, S. I., and Nilges, M. (2001) Automated assignment of ambiguous nuclear Overhauser effects with ARIA. *Methods Enzymol. 339*, 71–90.
28. Brünger, A. T., Adams, P. D., Clore, G. M., DeLano, W. L., Gros, P., Grosse-Kunstleve, R. W., Jiang, J. S., Kuszewski, J., Nilges, M., Pannu, N. S., Read, R. J., Rice, L. M., Simonson, T., and Warren, G. L. (1998) Crystallography & NMR system: A new software suite for macromolecular structure determination. *Acta Crystallogr. D54*, 905–921.
29. Kleywegt, G. J., Henrick, K., Dodson, E. J., and van Aalten, D. M. (2003) Pound-wise but penny-foolish: How well do micromolecules fare in macromolecular refinement? *Structure 11*, 1051–1059.
30. Laskowski, R. A., MacArthur, M. W., Moss, D. S., and Thornton, J. M. (1993) PROCHECK: A program to check the stereochemical quality of protein structures. *J. Appl. Crystallogr. 26*, 283–291.
31. Koradi, R., Billeter, M., and Wüthrich, K. (1996) MOLMOL: A program for display and analysis of macromolecular structures. *J. Mol. Graphics 14*, 51–55, 29−32.
32. DeLano, W. L. (2008) The PyMOL Molecular Graphics System, DeLano Scientific LLC, San Carlos, CA.
33. Holm, L., and Sander, C. (1996) Mapping the protein universe. *Science 273*, 595–603.
34. Farrow, N. A., Muhandiram, R., Singer, A. U., Pascal, S. M., Kay, C. M., Gish, G., Shoelson, S. E., Pawson, T., Forman-Kay, J. D., and Kay, L. E. (1994) Backbone dynamics of a free and phosphopeptide-complexed Src homology 2 domain studied by ^{15}N NMR relaxation. *Biochemistry 33*, 5984–6003.
35. Dosset, P., Hus, J. C., Blackledge, M., and Marion, D. (2000) Efficient analysis of macromolecular rotational diffusion from heteronuclear relaxation data. *J. Biomol. NMR 16*, 23–28.
36. Lipari, G., and Szabo, A. (1982) Model-free approach to the interpretation of nuclear magnetic resonance relaxation in macromolecules. 1. Theory and range of validity. *J. Am. Chem. Soc. 104*, 4546–4559.
37. Lipari, G., and Szabo, A. (1982) Model-free approach to the interpretation of nuclear magnetic resonance relaxation in macromolecules. 2. Analysis of experimental results. *J. Am. Chem. Soc. 104*, 4559–4570.
38. Loria, J. P., Rance, M., and Palmer, A. G. (1999) A relaxation-compensated Carr-Purcell-Meiboom-Gill sequence for characterizing chemical exchange by NMR Spectroscopy. *J. Am. Chem. Soc. 121*, 2331–2332.
39. Cavanagh, J., Fairbrother, W. J., Palmer, A. G., III, Skelton, N. J., and Rance, M. (1996) *Protein NMR Spectroscopy: Principles and Practice*, Academic Press, New York.
40. Laska, M., Galizia, C. G., Giurfa, M., and Menzel, R. (1999) Olfactory discrimination ability and odor structure-activity relationships in honeybees. *Chem. Senses 24*, 429–438.
41. Lautenschlager, C., Leal, W. S., and Clardy, J. (2007) Pheromone-binding protein binding nonpheromone ligands: Implications for pheromone recognition. *Structure 15*, 1148–1154.
42. Lartigue, A., Gruez, A., Briand, L., Blon, F., Bézirard, V., Walsh, M., Pernollet, J. C., Tegoni, M., and Cambillau, C. (2004) Sulfur single-wavelength anomalous diffraction crystal structure of a pheromone-binding protein from the honeybee *Apis mellifera L. J. Biol. Chem. 279*, 4459–4464.
43. Sandler, B. H., Nikonova, L., Leal, W. S., and Clardy, J. (2000) Sexual attraction in the silkworm moth: Structure of the pheromone-binding-protein-bombykol complex. *Chem. Biol. 7*, 143–151.
44. Horst, R., Damberger, F., Luginbuhl, P., Guntert, P., Peng, G., Nikonova, L., Leal, W. S., and Wüthrich, K. (2001) NMR structure reveals intramolecular regulation mechanism for pheromone binding and release. *Proc. Natl. Acad. Sci. U.S.A. 98*, 14374–14379.
45. Lee, D., Damberger, F. F., Peng, G., Horst, R., Guntert, P., Nikonova, L., Leal, W. S., and Wüthrich, K. (2002) NMR structure of the unliganded *Bombyx mori* pheromone-binding protein at physiological pH. *FEBS Lett. 531*, 314–318.
46. Lautenschlager, C., Leal, W. S., and Clardy, J. (2005) Coil-to-helix transition and ligand release of *Bombyx mori* pheromone-binding protein. *Biochem. Biophys. Res. Commun. 335*, 1044–1050.
47. Lartigue, A., Gruez, A., Spinelli, S., Rivière, S., Brossut, R., Tegoni, M., and Cambillau, C. (2003) The crystal structure of a cockroach pheromone-binding protein suggests a new ligand binding and release mechanism. *J. Biol. Chem. 278*, 30213–30218.
48. Mohanty, S., Zubkov, S., and Gronenborn, A. M. (2004) The solution NMR structure of *Antheraea polyphemus* PBP provides new insight into pheromone recognition by pheromone-binding proteins. *J. Mol. Biol. 337*, 443–451.
49. Zubkov, S., Gronenborn, A. M., Byeon, I. J., and Mohanty, S. (2005) Structural consequences of the pH-induced conformational switch in *A. polyphemus* pheromone-binding protein: Mechanisms of ligand release. *J. Mol. Biol. 354*, 1081–1090.
50. Kruse, S. W., Zhao, R., Smith, D. P., and Jones, D. N. (2003) Structure of a specific alcohol-binding site defined by the odorant binding protein LUSH from *Drosophila melanogaster*. *Nat. Struct. Biol. 10*, 694–700.
51. Wogulis, M., Morgan, T., Ishida, Y., Leal, W. S., and Wilson, D. K. (2006) The crystal structure of an odorant binding protein from *Anopheles gambiae*: Evidence for a common ligand release mechanism. *Biochem. Biophys. Res. Commun. 339*, 157–164.
52. Damberger, F. F., Ishida, Y., Leal, W. S., and Wüthrich, K. (2007) Structural basis of ligand binding and release in insect pheromone-binding proteins: NMR structure of *Antheraea polyphemus* PBP1 at pH 4.5. *J. Mol. Biol. 373*, 811–819.
53. Rivière, S., Lartigue, A., Quennedey, B., Campanacci, V., Farine, J. P., Tegoni, M., Cambillau, C., and Brossut, R. (2003) A pheromone-binding protein from the cockroach *Leucophaea maderae*: Cloning, expression and pheromone binding. *Biochem. J. 371*, 573–579.
54. Danty, E., Briand, L., Michard-Vanhée, C., Perez, V., Arnold, G., Gaudemer, O., Huet, D., Huet, J. C., Ouali, C., Masson, C., and Pernollet, J. C. (1999) Cloning and expression of a queen pheromone-binding protein in the honeybee: An olfactory-specific, developmentally regulated protein. *J. Neurosci. 19*, 7468–7475.
55. Vincent, F., Spinelli, S., Ramoni, R., Grolli, S., Pelosi, P., Cambillau, C., and Tegoni, M. (2000) Complexes of porcine odorant binding protein with odorant molecules belonging to different chemical classes. *J. Mol. Biol. 300*, 127–139.
56. Peng, T., Zintsmaster, J. S., Namanja, A. T., and Peng, J. W. (2007) Sequence-specific dynamics modulate recognition specificity in WW domains. *Nat. Struct. Mol. Biol. 14*, 325–331.
57. Bucci, B. K., Kruse, S. W., Thode, A. B., Alvarado, S. M., and Jones, D. N. (2006) Effect of n-alcohols on the structure and stability of the *Drosophila* odorant binding protein LUSH. *Biochemistry 45*, 1693–1701.
58. Pesenti, M. E., Spinelli, S., Bézirard, V., Briand, L., Pernollet, J. C., Tegoni, M., and Cambillau, C. (2008) Structural basis of the honey bee PBP pheromone and pH-induced conformational change. *J. Mol. Biol. 380*, 158–169.
59. Gouet, P., Courcelle, E., Stuart, D. I., and Metoz, F. (1999) ESPript: Analysis of multiple sequence alignments in PostScript. *Bioinformatics 15*, 305–308.

BI802300K